






# Photoplethysmographic Waveform and Pulse Rate Variability Analysis in Hyperbaric Environments

María Dolores Peláez-Coca , Alberto Hernando, María Teresa Lozano , Carlos Sánchez , David Izquierdo , and Eduardo Gil 

**Abstract**—The main aim of this work is to identify alterations in the morphology of the pulse photoplethysmogram (PPG) signal, due to the exposure of the subjects to a hyperbaric environment. Additionally, their Pulse Rate Variability (PRV) is analysed to characterise the response of their Autonomic Nervous System (ANS). To do that, 28 volunteers are introduced into a hyperbaric chamber and five sequential stages with different atmospheric pressures from 1 atm to 5 atm are performed. In this work, nineteen morphological parameters of the PPG signal are analysed: the pulse amplitude; eight parameters related to pulse width; eight parameters related to pulse area; and the two two pulse slopes. Also, classical time and frequency parameters of PRV are computed. Notable widening of the pulses width is observed in the stages analysed. The PPG area increases with pressure, with no significant changes when the initial pressure is recovered. These changes in PPG waveform may be caused by an increase in the systemic vascular resistance as a consequence of vasoconstriction in the extremities, suggesting a sympathetic activation. However, the PRV results show an augmented parasympathetic activity and a reduction in the parameters that characterise the

sympathetic response. So, only a sympathetic activation is detected in the peripheral region, as reflected by PPG morphology. The information regarding the ANS and the cardiovascular response that can be extracted from the PPG signal, as well as its compatibility with wet conditions make this signal the most suitable for studying the physiological response in hyperbaric environments.

**Index Terms**—Autonomic nervous system, hyperbaric environments, photoplethysmographic waveform, pulse rate variability, pulse width.

## I. INTRODUCTION

**A**N IMMERSION in a hyperbaric environment represents a considerable physiological challenge, since our body has to adapt to the conditions of this environment to maintain homeostasis. [1]. The ability of physiological systems to respond to the challenge of immersion highly depends on heart rate and blood pressure control systems. Particularly, the Autonomic Nervous System (ANS) exhibits a fast response to blood pressure changes motivated by immersion [2]. The analysis of Heart Rate Variability (HRV) is the non-invasive measurement most commonly used to evaluate both the activity of the ANS and the balance between its two branches: sympathetic and parasympathetic. The classical analysis of the HRV [3] considers the power in the low-frequency band (LF, 0.04–0.15 Hz) as a measurement of both sympathetic and parasympathetic systems, whereas the power in the high-frequency band (HF, 0.15–0.4 Hz) is considered a measurement of parasympathetic activity alone. The ratio between LF and HF ( $R_{LF/HF}$ ) is used to estimate the balance between the two branches. The response of the ANS has been analysed in multiple works simulating conditions of high atmospheric pressures in hyperbaric chambers, without the need of actually immersing people in water [4]–[6]. Their results point to an increase in the power related to the HF band, associated with an increase in the parasympathetic activity [4]–[6]. Another conclusion of the studies in hyperbaric environments is the reduction of the heart rate [4], [5], although in one of them this trend was not observed [6]. Bradycardia in hyperbaric environment has several causes, but it seems that the increase in the partial pressure of oxygen is the main cause [7], [8]. Furthermore, in normal tissues, the primary action of oxygen is to cause general vasoconstriction (especially in the kidneys,

Manuscript received April 28, 2020; revised July 2, 2020 and August 19, 2020; accepted August 24, 2020. Date of publication September 1, 2020; date of current version May 11, 2021. This work was supported in part by *Ministerio de Ciencia, Innovación y Universidades*, in part by FEDER through the projects PGC2018-095936-B-I00 and RTI2018-097723-B-I00, in part by *Centro Universitario de la Defensa* (CUD) under the projects UZCUD2019-TEC-01 and CUD2019-10, and in part by Aragón Government and European Regional Development Fund through *Grupos de Referencia* BSICoS (Biomedical Signal Interpretation & Computational Simulation, T39-20R) and GTF (Grupo de Tecnologías Fotónicas T20-20R). The computation was performed by the ICTS NANBIOSIS, specifically by the High Performance Computing Unit of CIBER-BBN at University of Zaragoza. (Corresponding author: María Dolores Peláez-Coca.)

María Dolores Peláez-Coca, Alberto Hernando, María Teresa Lozano, and Carlos Sánchez are with Centro Universitario de la Defensa (CUD), Zaragoza, Spain, and also with BSICoS group, Aragón Institute of Engineering Research (I3A), IIS Aragón, University of Zaragoza, 50009 Zaragoza, Spain (e-mail: mdpelaez@unizar.es; ahersanz@unizar.es; maytelo@unizar.es; cstapia@unizar.es).

David Izquierdo is with Centro Universitario de la Defensa (CUD), Zaragoza, Spain and also with Photonic Technologies Group (GTF), Aragón Institute of Engineering Research (I3A), Universidad de Zaragoza, Zaragoza, Spain (e-mail: d.izquierdo@unizar.es).

Eduardo Gil is with Centro de Investigación Biomédica en Red Bioingeniería, Biomateriales y Nanomedicina (CIBER-BBN), 28029 Madrid, Spain, and also with BSICoS group, Aragón Institute of Engineering Research (I3A), IIS Aragón, University of Zaragoza, 50009 Zaragoza, Spain (e-mail: edugilh@unizar.es).

Digital Object Identifier 10.1109/JBHI.2020.3020743

skeletal muscle, brain and skin) [9]. After removal from the hyperbaric oxygen environment, the tissue oxygen tension may remain elevated for a variable period, which can vary from minutes to a few hours, depending on tissue perfusion [10], [11]. An examination of the cardiovascular and nervous systems, before and after exposure to 4 atm in a hyperbaric chamber, showed a decrease in heart rate, an increase in mean and diastole blood pressure, and an increase in total peripheral resistance and in parasympathetic heart nerves activity. This suggests an increase in heart afterload with a decrease in heart activity within almost one hour after hyperbaric exposure [12].

An alternative way of measuring the activity of the ANS is the Pulse Rate Variability signal (PRV), extracted from the photoplethysmographic signal (PPG) [13]. Some studies, performed at a pressure of 1 atm, concluded that HRV and PRV contained the same information of the ANS activity [14]–[16]. The results of our previous study conducted with subjects in a hyperbaric environment verified that this relationship was maintained in pressures up to 5 atm [2]. It was also shown that time-derived parameters of HRV/PRV indicated a reduction in heart rate correlated with time spent in a hyperbaric environment, even after a decrease in pressure [2]. On the other hand, regarding frequency parameters, HF power was positively correlated with changes in pressure, while the sympathetic markers showed a decrease ( $P_{LFn}$ , normalized power in the LF band, and  $R_{LF/HF}$ ) [2].

The PPG signal reflects the movement of the blood in the blood vessels, which is mainly affected by heartbeating, as well as by hemodynamics and changes in the arteriole properties. These effects cause distortions in the pulse waveform that have been related to physiological changes in the subjects. A reduction in the pulse amplitude may be directly attributable to a loss of central arterial pressure or to the arteriolar constriction that perfuse the skin, which is related to an activation of the sympathetic system of the subject [17]. Other studies suggest that the PPG width correlates better with the systemic vascular resistance than the PPG amplitude [18]. Another interesting parameter is the pulse area, dividing it into two sub-areas separated by the dicrotic point (inflection point on the pulse downward slope). The ratio between both sub-areas is a parameter related to total peripheral resistance [19].

A wide variety of morphological features of the PPG signal can be found in the literature, in non-hyperbaric environments. The width and amplitude of the PPG pulses have shown greater sensitivity for the identification of a low activation of the sympathetic system, due to mental stress states, than the classic frequency parameters of HRV and PRV ( $P_{LFn}$  and  $R_{LF/HF}$ ) [20]. In the study by Li *et al.* [21], twenty-one features related to the morphology of the PPG signal allowed the non-invasive detection of physical stress states. Also, changes in the PPG amplitude have been associated with changes in the baroreflex response due to postural changes [22] or with hypovolemia episodes [23].

The exposure of subjects to a hyperbaric environment causes a physiological response (blood distribution changes, augmented cardiac output, low heart rate, HF band alterations, etc.) [2]. These subjects also experience a higher density of breathing gases, changes in blood distribution, increased cardiac output, augmented resistance to movement, alterations in temperature,

etc., which have an impact on the PPG morphology. In our previous work, the effects of a hyperbaric environment on the amplitude, width and slope of the PPG pulse were studied [24]. The results showed only a significant increase in pulse width with increasing pressure. However, the method used to estimate these parameters generates an overestimate of the width and an underestimation of the slope of the PPG pulse. In this work this overestimation problem is corrected and a greater diversity of morphological parameters have been extracted. In addition, PPG shows three important advantages for its use in hyperbaric environments. The first one is the low price of the PPG recording device, which is also fully compatible with wet environments, such as diving activities. The second one is that this device is commonly used in clinical practice and can be placed in different parts of the body. The last one is that the PPG signal allows measuring blood oxygen saturation. For all these reasons, an analysis of the PRV and the PPG waveform is proposed in this paper, with the aim of identifying features that show significant changes in the ANS response of subjects exposed to variable hyperbaric environments.

## II. MATERIALS

A total of 28 subjects (25 males and 3 females), with a mean age of  $28.5 \pm 6.2$  years were recorded in the study. All subjects were recorded inside a hyperbaric chamber of the *Hospital General de la Defensa en Zaragoza*, after receiving the approval of the *Comité de ética de la investigación con medicamentos de la inspección general de sanidad de la Defensa* (Ethics Committee of Research with Medicines, attached to the Surgeon General of the Undersecretary of Defense), and the participant information sheet and informed consent were signed. The protocol inside the hyperbaric chamber had a duration of about two hours. Five different stages involving 5 min stops at 1 atm (1D, sea level), 3 atm (3D, simulating 20 metres depth) and 5 atm (5, simulating 40 meters depth), and subsequently returning to 3 atm (3A) and 1 atm (1A) were performed, defining the stages of the study. The letter D or A refers to descent or ascent stage, respectively. Most of the time was spent in the decompression stops between 3 atm and 1 atm, as recommended in standard decompression tables. Subjects stayed relaxed and sitting comfortably, and the chamber was correctly ventilated throughout the protocol in an attempt to avoid major changes in temperature and humidity. Subjects remained in silence and without performing movements during control stops. Several measures to reduce the stress that the test might induce were previously taken: the subjects are expert divers, they perform a relaxation exercise before the test, a test to measure trait and state anxiety is also performed (STAI test) whose results showed no anxiety in any subject, etc. More details of the database are given in our previous study [2]. In this study, only the last four minutes of each stage were used in order to avoid measuring transient effects, due to the adaptation of the subject to the change in atmospheric pressure.

The recordings were done using the Nautilus device developed by the University of Kaunas, Lithuania [25]. This device allows recording the PPG signal at a sampling frequency ( $f_s$ ) of 1000 Hz in a finger by a transmissive sensor using a 650 nm (red) wavelength, the ECG signal with three leads ( $f_s = 2000$  Hz),

TABLE I

HYPERBARIC CHAMBER TEMPERATURE AT EACH STAGE. RESULTS SHOWN AS MEDIAN/INTERQUARTILE RANGE VALUES

	1D	3D	5	3A	1A
°C	31.3/3.2	33.7/2.5	34.3/2.4	31.8/2.8	32.8/2.8

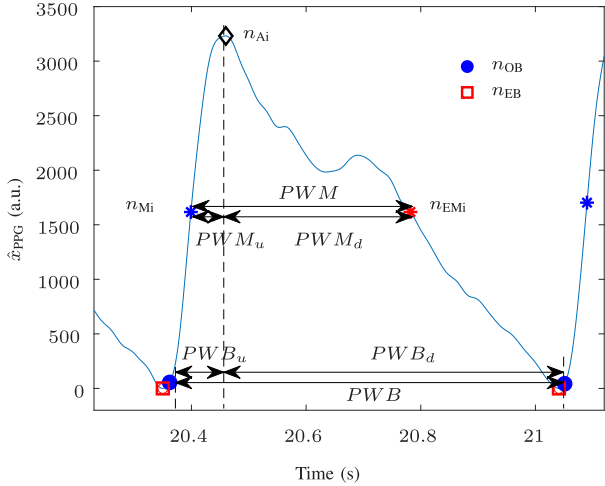


Fig. 1. Location of the onset  $n_{OB}$ , end  $n_{EB}$ , medium  $n_M$ , medium in catarcotic phase  $n_{EM}$  and apex  $n_A$  points, necessary to compute PPG signal morphological parameters.

ambient temperature (accuracy  $\pm 0.1$  °C,  $f_s = 50$  Hz), and pressure ( $f_s = 250$  Hz). The PPG sensor is located in the middle finger of the non-dominant hand. Prior to stage 1D, the subjects remain between 20 to 30 minutes in a room connected to the hyperbaric chamber, to acclimatize to the temperature of that room and to reduce the stress impact for the experiment. There, the subjects complete and sign the informed consent and the Nautilus is placed on them. The median and interquartile range values of the hyperbaric chamber temperature at each stage are shown in Table I. The Nautilus also allows including marks in all signals, synchronously. These marks were used to segment the signal intervals corresponding to the five studied stages.

### III. METHODS

#### A. Time Parameters of the PRV Signal

A low-pass FIR filter was firstly applied to the PPG signal, with red wavelength, to estimate baseline in order to remove it from the signal (cut-off frequency of 0.07 Hz) [26]. Another low-pass FIR filter, with cut-off frequency of 35 Hz, was applied over the PPG signal to remove the high frequency noise [27]. The resulting signal was named as  $x_{PPG}(n)$ .

Artefactual pulses in the preprocessed PPG signal were suppressed by using the artefact detector described in [28]. Then, the apex ( $n_{Ai}$ ), the basal ( $n_{Bi}$ ) and the medium ( $n_{Mi}$ ) points of the  $i$ -th PPG pulse were automatically detected using an algorithm based on a low-pass differentiator filter [29]. These points are highlighted in Fig. 1. The medium points were considered the fiducial points in the PPG because of their robustness for computing the pulse to pulse (PP) time series as the difference between consecutive  $n_{Mi}$  [30].

Four time parameters were computed from the PP time series, and then the mean of these parameters in the last four minutes for each stage were obtained (1D, 3D, 5, 3A and 1A):

- $\overline{NN}$ : median of the Normal-to-Normal (NN) intervals between the fiducial points (measure units: s);
- $\overline{IQR}$ : interquartile range as a measure of statistical dispersion (measure units: s);
- $\overline{RMSSD}$ : root mean square of the successive differences between adjacent NN intervals (measure units: s);
- $\overline{pNN50}$ : number of pairs of successive NN that differ by more than 50 ms, divided by the total number of NN (measure units: %).

#### B. Frequency Parameters of the PRV Signal

With the PP time series, the instantaneous pulse rate (PR) signal ( $d_{PR}(n)$ ) was obtained at 4 Hz using cubic spline interpolation. The basis for the analysis of the ANS is the integral pulse frequency modulation model [31]:

$$d_{PR}(n) = \frac{1 + \mathfrak{m}(n)}{T(n)}, \quad (1)$$

with  $\mathfrak{m}(n)$  being the modulating signal carrying the information from the ANS and  $T(n)$  the mean pulse period, considered the variations of the term  $1/T(n)$  are slower than those of the term  $\mathfrak{m}(n)/T(n)$  in the model.

Then, a time-varying mean PR, ( $d_{PRM}(n)$ ), was obtained by low-pass filtering  $d_{PR}(n)$ , with a cut-off frequency of 0.03 Hz:

$$d_{PRM}(n) = \frac{1}{T(n)} \quad (2)$$

Later on, PRV signal ( $d_{PRV}(n)$ ) was obtained as:

$$d_{PRV}(n) = d_{PR}(n) - d_{PRM}(n) \quad (3)$$

Finally,  $\mathfrak{m}(n)$  was obtained by correcting  $d_{PRV}(n)$  by  $d_{PRM}(n)$ :

$$\mathfrak{m}(n) = \frac{d_{PRV}(n)}{d_{PRM}(n)} \quad (4)$$

Four frequency parameters were calculated based on the power spectral distribution (PSD) analysis of the modulating signal  $\mathfrak{m}(n)$ . The 4-min-duration recording for every atmospheric pressure stage was considered stationary. Therefore, classic frequency domain indices were computed for the  $\mathfrak{m}(n)$  signal using Welch's power spectral density estimation, with seven 1-min-duration Hamming windows and an overlap of 50%. In summary, the following frequency parameters were defined in each stage (1D, 3D, 5, 3A and 1A):

- $P_{LF}$ : power in the LF band (0.04–0.15 Hz; measure units: arbitrary units, a.u.);
- $P_{HF}$ : power in the HF band (0.15–0.4 Hz; measure units: a.u.);
- $P_{LF_n}$ : power in the LF band normalized with respect to the powers in the LF and HF bands (measure units: n.u., normalized units):  $P_{LF_n} = P_{LF}/(P_{LF} + P_{HF})$ ;
- $R_{LF/HF}$ : ratio between LF and HF power (measure units: n.u.):  $R_{LF/HF} = P_{LF}/P_{HF}$ .

### C. Morphological Parameters of the PPG Signal

The PPG waveform is usually splitted in two phases: the upward and downward segments of the pulse (anacrotic and catacrotic phase, respectively). The first phase primarily concerns systole, and the second phase diastole and wave reflections from the periphery [17].

In this work, nineteen morphological parameters of the PPG signal were considered. To extract these parameters, the PPG signal was transformed so that it only has positive values. To do this, a cubic spline interpolation over the points with the least amplitude of each pulse was subtracted from the PPG signal, obtaining  $\hat{x}_{PPG}$  signal.

To define the morphological parameters, six different characteristic points of the PPG pulse were used. These characteristic points are highlighted in Fig. 1. The first three characteristic points were the apex ( $n_{Ai}$ ), the basal ( $n_{Bi}$ ) and the medium ( $n_{Mi}$ ) points of the  $i$ -th PPG, defined in Section III-A.

The next two characteristic points were the onset ( $n_{OBi}$ ) and end points ( $n_{EBi}$ ).  $n_{OBi}$  was estimated similarly to the onset point in Lázaro *et al.* [27], but using the  $\hat{x}_{PPG}(n)$  signal without the additional low-pass filter, which would cause an overestimation of the pulse width.

The  $n_{EBi}$  was estimated based on the assumption that this point, in the PPG signal, must have an amplitude similar to  $n_{OBi}$ , due to the elimination of the PPG baseline in the preprocessing. Thus,  $n_{EBi}$  was estimated in a similar way as the end point in [27], but without filtering the PPG signal and looking for the point with slope closest to the slope  $\eta x'_{PPG}(n_{Ui})$  in the interval  $[n_{oxi}, n_{exi}]$ .  $\eta x'_{PPG}(n_{Ui})$  represents a beat variable threshold dependent on the minimum slope, reached at point  $n_{Ui}$ .

$n_{oxi}$  and  $n_{exi}$  were determined by the following equations:

$$\begin{aligned} n_{oxi} &= D_i(1), \\ n_{exi} &= \min \{n_{Ai} + 1.3f_s, n_{Ai+1}\}, \end{aligned} \quad (5)$$

where

$$D_i(n) = \{n \mid \hat{x}_{PPG}(n) \leq (\hat{x}_{PPG}(n_{OBi}) + \delta(\hat{x}_{PPG}(n_{Ai}) - \hat{x}_{PPG}(n_{Bi}))) \forall n \in [n_{Ai}, n_{exi}]\}. \quad (6)$$

A value of  $\delta = 0.1 + \alpha \cdot 0.1$ , where  $0 \leq \alpha \leq 9$  and  $\alpha \in \mathbb{N}$  was considered. The value of  $\alpha$  is the smallest value that makes the number of elements in the interval  $D_i$  greater than 50.

The multiplicative factor of  $f_s$  that was used in the computation of  $n_{exi}$  was considered as 1.3 s to adapt the estimation to the characteristics of the population, which contains subjects with low cardiac frequencies.

$\eta$  factor was 0.03 to detect  $n_{EBi}$  and 0.15 to detect  $n_{OBi}$ , since the pulse slope in catacrotic phase is five times shallower than in the anacrotic phase, in this population. This factor was estimated considering the beginning and the end of the pulse as the points with less amplitude in the intervals  $[n_{Ai} - 0.6f_s, n_{Ai}]$  and  $[n_{Ai}, n_{Ai} + 1.3f_s]$ , respectively.

The last characteristic point was the point of the catacrotic phase of the pulse  $i$ -th, with the same amplitude as  $\hat{x}_{PPG}(n_{Mi})$ .

This point was named as  $n_{EMi}$  and was estimated as:

$$\begin{aligned} n_{EMi} &= \arg \min_n \{|\hat{x}_{PPG}(n_{Mi}) - \hat{x}_{PPG}(n)| \\ &\forall n \in [n_{Ai}, n_{yi}]\}, \end{aligned} \quad (7)$$

where  $n_{yi} = \min\{n_{OBi+1}, n_{Ai} + 0.6f_s\}$ .

The morphological parameters extracted, based on these characteristic points, can be divided into four categories:

1) **Amplitude of PPG Pulse:** the first parameter was the amplitude of the PPG pulse (PA), which was estimated based on the following equation using the apex and basal points ( $n_{Ai}$  and  $n_{Bi}$ ):

$$PA(i) = \hat{x}_{PPG}(n_{Ai}) - \hat{x}_{PPG}(n_{Bi}) \quad (8)$$

2) **Width of PPG Pulse:** The times elapsed between different points of the pulse were the origin of eight of the morphological parameters. The first one was the time between the onset point ( $n_{OBi}$ ) and the end point ( $n_{EBi}$ ) (Fig. 1). This pulse width was named as PWB, where  $B$  refers to the base of the pulse, and it was estimated as:

$$PWB(i) = \frac{1}{f_s}(n_{EBi} - n_{OBi}) \quad (9)$$

The pulse width, measured at half height of the PPG pulse (PWM), was also included among the morphological parameters.  $M$  refers to the medium points ( $n_{Mi}$  and  $n_{EMi}$ ). This width was estimated as:

$$PWM(i) = \frac{1}{f_s}(n_{EMi} - n_{Mi}) \quad (10)$$

The next four pulse width parameters were defined based on the previous ones, in the anacrotic and catacrotic phases, with the point of maximum amplitude of the pulse,  $n_{Ai}$ , separating them. These parameters were estimated as:

$$\begin{aligned} PWB_u(i) &= \frac{1}{f_s}(n_{Ai} - n_{OBi}) & PWB_d(i) &= \frac{1}{f_s}(n_{EBi} - n_{Ai}) \\ PWM_u(i) &= \frac{1}{f_s}(n_{Ai} - n_{Mi}) & PWM_d(i) &= \frac{1}{f_s}(n_{EMi} - n_{Ai}) \end{aligned} \quad (11)$$

where the subscript  $u$  means upslope associated to anacrotic phase while the subscript  $d$  means downslope associated to catacrotic phase.

To study the relationship between the anacrotic and the catacrotic phase, the ratios of the widths between these phases were included among the selected parameters:

$$PWB_r(i) = \frac{PWB_d(i)}{PWB_u(i)} \quad PWM_r(i) = \frac{PWM_d(i)}{PWM_u(i)} \quad (12)$$

3) **Slopes of PPG Pulse:** The slopes of the anacrotic (upward) and catacrotic (downward) phases of each PPG pulse, simplified as the Pulse Slope (PS), were computed as follows, based on the amplitude and widths of each phase:

$$\begin{aligned} PS_u(i) &= \frac{\hat{x}_{PPG}(n_{Ai}) - \hat{x}_{PPG}(n_{OBi})}{PWB_u(i)} \\ PS_d(i) &= \frac{\hat{x}_{PPG}(n_{Ai}) - \hat{x}_{PPG}(n_{EBi})}{PWB_d(i)} \end{aligned} \quad (13)$$

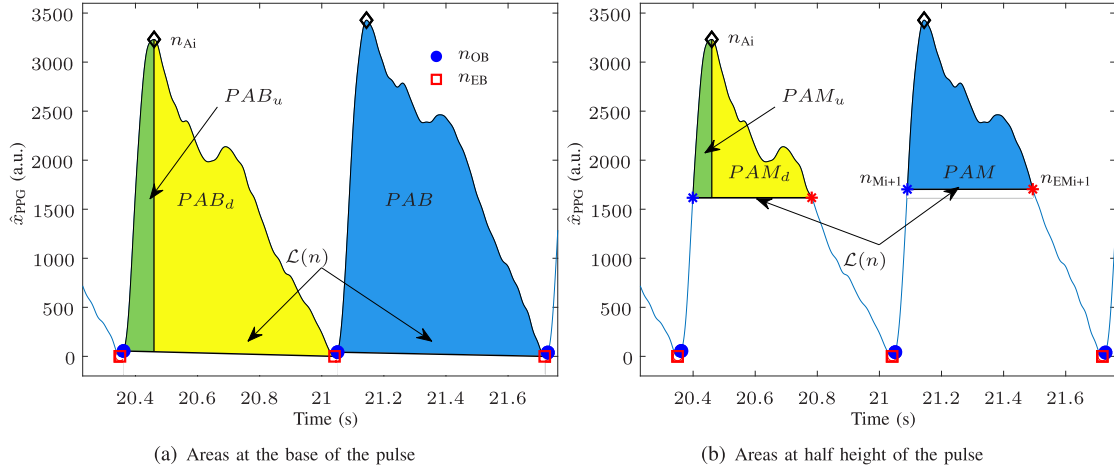


Fig. 2. Areas under the PPG curve with baseline of the areas at the pulse base (top figure) and at half height of the pulse (bottom figure).  $\mathcal{L}(n)$  is the equation of the straight line defined through the start and end points of the areas.

4) *Areas of PPG Pulse*: The last eight morphological parameters were the areas under the PPG curve limited by the points  $n_{OBi}$ ,  $n_{Mi}$ ,  $n_{Ai}$ ,  $n_{EMi}$  and  $n_{EBi}$ , and the ratio of the two areas in anacrotic and catacrotic phases. Fig. 2 shows an example of the estimated areas for two pulses of the PPG signal.

The area under the PPG curve was estimated as:

$$\mathcal{A}(i) = \sum_{n=a}^b (\hat{x}_{PPG}(n) - \mathcal{L}(n)); \quad (14)$$

where  $\mathcal{L}$  is the equation of the straight line defined through the points  $(a, \hat{x}_{PPG}(a))$  and  $(b, \hat{x}_{PPG}(b))$ .

Finally, the PPG areas were estimated as:

$$\begin{aligned} PAB(i) &= \{\mathcal{A}(i) : a = n_{OBi}, b = n_{EBi}\} \\ PAB_u(i) &= \{\mathcal{A}(i) : a = n_{OBi}, b = n_{Ai}\} \\ PAB_d(i) &= \{\mathcal{A}(i) : a = n_{Ai}, b = n_{EBi}\} \\ PAM(i) &= \{\mathcal{A}(i) : a = n_{Mi}, b = n_{EMi}\} \\ PAM_u(i) &= \{\mathcal{A}(i) : a = n_{Mi}, b = n_{Ai}\} \\ PAM_d(i) &= \{\mathcal{A}(i) : a = n_{Ai}, b = n_{EMi}\} \end{aligned} \quad (15)$$

The ratios of the two areas in catacrotic and anacrotic phases were estimated as:

$$PAB_r(i) = \frac{PAB_d(i)}{PAB_u(i)} \quad PAM_r(i) = \frac{PAM_d(i)}{PAM_u(i)} \quad (16)$$

A median filter was used to identify outliers in the calculated morphological parameters [32], where every sample outside the range  $[median \pm G \cdot std]$  of the  $N_g$  previous data was removed. In this study,  $G = 5$  and  $N_g = 25$ .

In summary, based on the characteristic points of each pulse of the PPG signal (Fig. 1), the morphological parameters shown in Table II were defined as the mean of the four minutes of each stage (1D, 3D, 5, 3A and 1A).

TABLE II

SUMMARY OF THE MORPHOLOGICAL PARAMETERS EXTRACTED. (a.u. ARBITRARY UNITS, n.u. NORMALIZED UNITS)

Groups	Parameters	Measure units
Amplitude	$\bar{PA}$	a.u.
Widths	$\overline{PWB}, \overline{PWM}, \overline{PWB}_u,$ $\overline{PWB}_d, \overline{PWM}_u, \overline{PWM}_d$	s.
	$\overline{PWB}_r, \overline{PWM}_r$	n.u.
Slopes	$\overline{PS}_u, \overline{PS}_d$	a.u.
Areas	$\overline{PAB}, \overline{PAM}, \overline{PAB}_u,$ $\overline{PAB}_d, \overline{PAM}_u, \overline{PAM}_d$	a.u.
	$\overline{PAB}_r, \overline{PAM}_r$	n.u.

#### D. Statistical Analysis

In order to minimize the effects of the intersubject variability, the Relative Change (RC) of each parameter ( $\mathcal{Y}$ ) with respect to the reference stage (1D), for each studied stage, was calculated as a percentage:

$$\mathcal{R}(\mathcal{Y}_S) = \frac{\mathcal{Y}_S - \mathcal{Y}_{1D}}{\mathcal{Y}_{1D}} \times 100, \quad (17)$$

where  $S$  can be 3D, 5, 3A or 1A.

The Shapiro-Wilk test was used to check normality of the ratios  $\mathcal{R}(\mathcal{Y}_S)$ . When the normal distribution of one ratio was verified, the t-Student paired test was applied. When not, the Wilcoxon paired test was applied. A  $p$ -value  $< \alpha$  defines significance in value with respect to basal state 1D, where the significance level  $\alpha$  can be 0.05, 0.01 or 0.001. This test allows identifying significant differences in each parameter, for each stage with respect to the basal state. Finally, a test using Anova statistics with Bonferroni correction for multiple comparisons was applied to assess the differences between the estimated RCs of the four stages. When the normal distribution of one RC of the considered group was not verified, a Friedman test was applied instead of the Anova test. These tests were applied

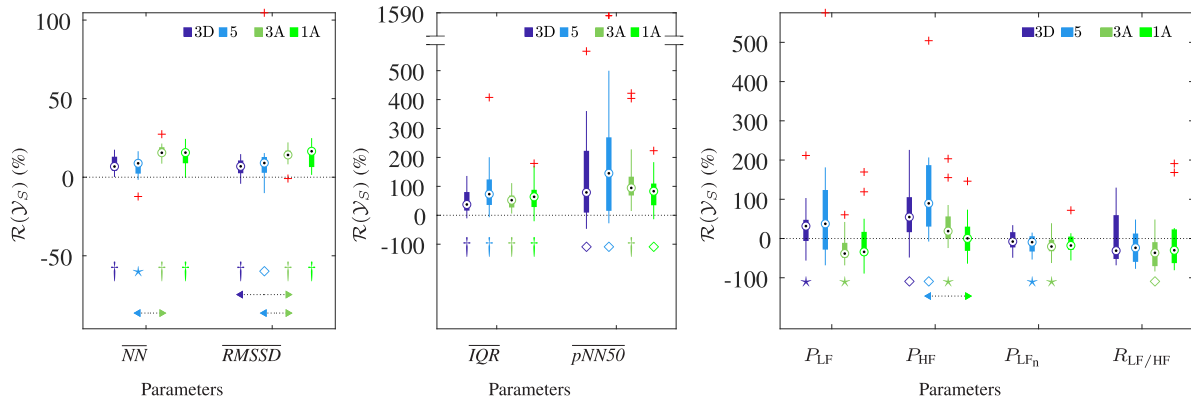


**Fig. 3.** Boxplots of the frequency and time parameters of the PRV. The significance level  $\alpha$  of the t-Student or Wilcoxon test is indicated with  $\star$  for  $\alpha = 0.05$ ,  $\diamond$  for  $\alpha = 0.01$  and  $\dagger$  for  $\alpha = 0.001$ . The arrows indicate statistically significant differences between compared groups using Anova or Friedman statistics with the Bonferroni correction for multiple comparisons test when the median value of one stage (arrow start) is significantly higher or lower than the other (arrow end). The colours of the start and end of the arrows indicate the stages analysed.

to each parameter and between the four stages with pressure increase (3D, 5, 3A and 1A).

#### IV. RESULTS

The population used in this study comprises 28 subjects whose PPG signal was recorded in five stages. Twenty-seven parameters were extracted from this signal: eight from the PRV signal and nineteen from the morphology of the PPG pulse. Data for one subject are only available for stages 1D, 3D and 5 as the recording suddenly stopped, thus meaning that the final two stages could not be recorded. Two other subjects present a very noisy signal in stage 1A. Therefore, there are 28 subjects for 1D, 3D and 5; 27 subjects for 3A; and 25 subjects for 1A.

##### A. Time and Frequency Parameters of the PRV Signal

Respiratory rate modifies the spectral power of the PRV signal. Thus, respiratory rates lower than 0.15 Hz or greater than 0.4 Hz may result in an overestimation of the power in the LF band or an underestimation of the power in the HF band, respectively. The analysis of the respiratory rate, and its effect on the PRV, was carried out in our previous study with this same database [2]. As a result, several subjects were discarded from various stages of the test, and considering the normalization with respect to the stage 1D in this study, the final number of subjects in each stage for time-frequency parameters was: 15 subjects in 3D, 13 subjects in 5, 15 subjects in 3A and 13 subjects in 1A.

Fig. 3 shows the distribution of each time-frequency parameter along the various stages. As regards time parameters, their values increase significantly with respect to basal state 1D. The frequency parameters show a significant increase in the  $P_{HF}$ , in stages 3D, 5 and 3A, while a decreases in  $P_{LFn}$  are mainly observed for stages 5 and 3A. The  $P_{LF}$  shows significant changes in stage 3D and 3A. These variations are consistent with an augmented activity of the parasympathetic branch of the ANS, together with a reduction in the activity of the sympathetic branch.

##### B. Morphological Parameters of the PRV Signal

Fig. 4(a) and (b) show significant increases in all stages for the parameters  $\overline{PWB_u}$ ,  $\overline{PWM}$  and  $\overline{PWM_u}$ , with respect to 1D stage. Similar results are observed in the area parameters (Fig. 4(c) and (d)), except for stage 1A. Significant changes are also observed in stages 3D, 5 and 3A, for the ratios between catarcotic and anarcotic phases of width and area parameters of the pulse, except for  $\overline{PAM_r}$ . Regarding the slopes (Fig. 4(e)), a significant decrease is observed in the ascending stages, respect 1D stage for  $\overline{PS_u}$ . Additionally, significant differences are found between stages 3D and 5, compared to stage 1A, in  $\overline{PA}$ ,  $\overline{PS_u}$  and  $\overline{PS_d}$ . These parameters maintain a reduction of around 40% of the basal state after recovering the pressure of 1 atm.  $\overline{PAB_u}$  and  $\overline{PS_d}$  parameters are the only ones that show significant changes in the stages with increased pressure, compared to the two stages at 1 atm, 1D and 1A. Note that the parameters extracted from the anarcotic phase of the pulse seem to follow the changes in atmospheric pressure better than the other morphological parameters.

#### V. DISCUSSION

In this work, the PPG signal of 28 subjects was recorded in five hyperbaric stages, from 1 atm to 5 atm (descent), and back to 1 atm (ascent), with stops at 3 atm in both descent and ascent. Twenty-seven parameters were extracted: eight from the PRV signal and nineteen from the morphology of the PPG pulse (Table II). The ANS control is complex, in a previous work a comparison based on ECG and PPG signals was performed and the conclusion was that the information that can be extracted from the ECG is highly correlated with that of the PPG [2]. The present work is focused on the latter due to its implicit advantages and thinking about monitoring using wearables. The study has been extended with the morphological analysis of PPG pulse that adds value to the PRV, which presented with similar results to the HRV based on ECG. The RCs of PRV parameters were calculated with respect to the reference stage

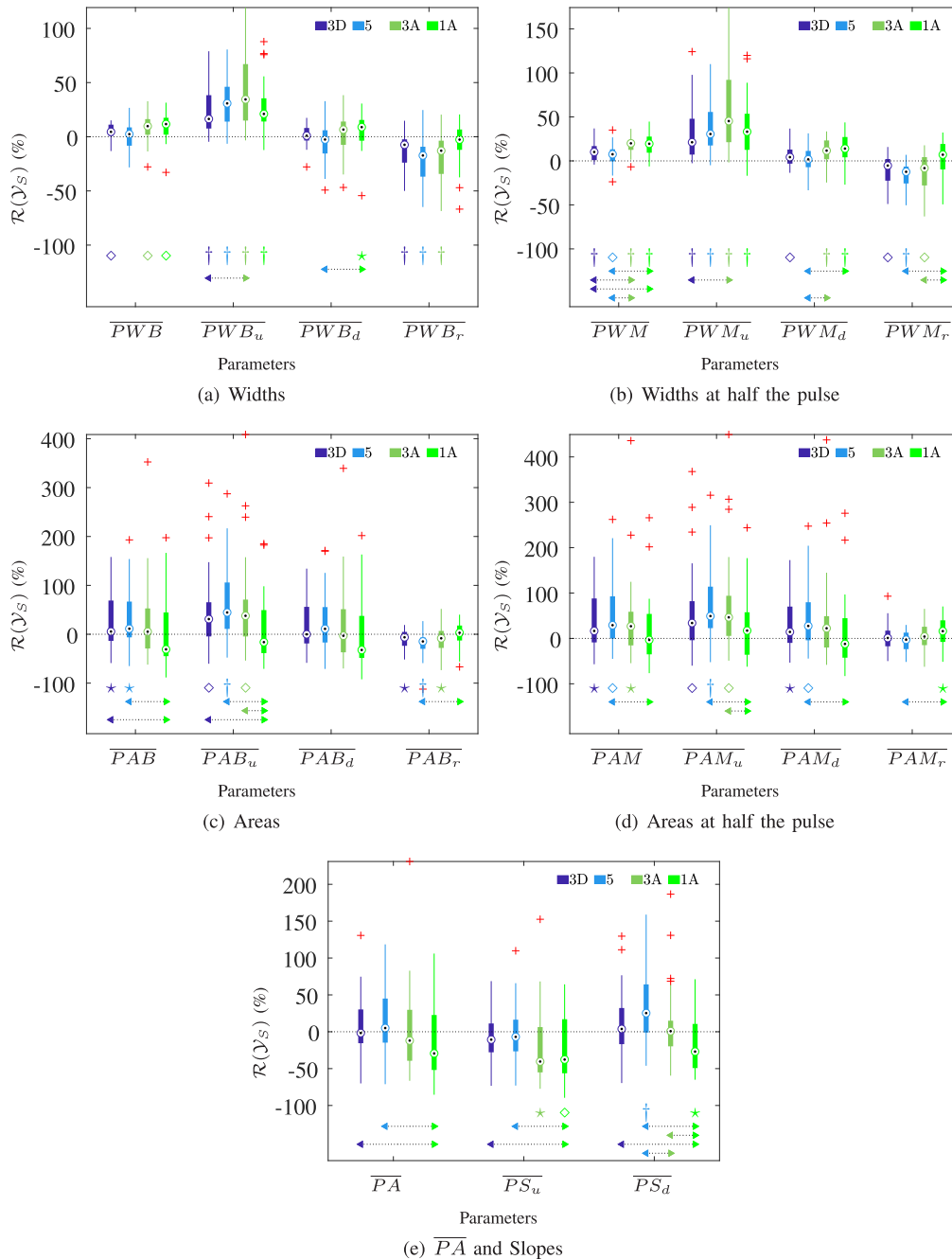


**Fig. 4.** Boxplots of the morphological parameters extracted from the PPG signal. The significance level  $\alpha$  of the t-Student or Wilcoxon test is indicated with  $\star$  for  $\alpha = 0.05$ ,  $\diamond$  for  $\alpha = 0.01$  and  $\dagger$  for  $\alpha = 0.001$ . The arrows indicate statistically significant differences between compared groups using Anova or Friedman statistics with the Bonferroni correction for multiple comparisons test when the median value of one stage (arrow start) is significantly higher or lower than the other (arrow end). The colours of the start and end of the arrows indicate the stages analysed.

(Equation 17). This allowed us to identify significant changes in some parameters, which were not appreciable without referencing the values to the baseline state of the subjects. This was the case of the significant increase observed in the  $P_{HF}$  in stages 3D, 5 and 3A, as well as the decrease observed in the  $P_{LFn}$  in stages 5 and 3A (Fig. 3).  $P_{HF}$  increased with pressure, while no significant changes were observed in stage 1A, which suggests that the  $P_{HF}$  of the subjects returns to its basal state.  $P_{HF}$  seems to respond quickly to changes in pressure, recovering

its baseline at 1A. These changes were observed in [2], but only for stage 5, not for intermediate stages. Therefore, the RC of the parameters with respect to the baseline stage could be essential in the analysis of the results. Furthermore, the time parameters showed significant changes with the time elapsed in a hyperbaric environment, without recovering the baseline state at 1A.

Regarding the morphological parameters, the first challenge was to improve the identification of the onset and end points of the pulse, with respect to previous works [20], [24]. The

estimation of the onset ( $n_{OBi}$ ) and end ( $n_{EBi}$ ) points was based on an algorithm whose objective was to estimate the respiratory rate through combining information extracted from the derived respiration signals for PPG, including the pulse width [27]. While the anacrotic phase of PPG pulse is abrupt, with a steep slope, the catacrotic phase is irregular, with many slope changes, and the presence of the diastolic peak and the dicrotic notch, which makes the estimation of the end of the pulse difficult. To palliate this difficulty, in [27] a low-pass filter was applied, which softens these irregularities, but introduces an overestimation in the width of the pulse. This overestimation is similar in all the pulses and does not suppose a disadvantage for the correct estimation of the respiratory rate of the subject. In the present work, pulse widths were compared in different hyperbaric stages and between different subjects. So, this overestimation in the width would not remain uniform in all the signals analysed, and therefore the filtering of the PPG signal was removed. Without this filtering, the algorithm by Lázaro *et al.* [27] could confuse the dicrotic notch with the pulse end point.  $n_{OBi}$  points were estimated without low-pass filtering the PPG signal, since the pronounced and uniform slope of the anacrotic phase of the pulse allows the estimation algorithm to work optimally. However, for the estimation of  $n_{EBi}$ , a redefinition of the search interval of the point was introduced. Since the baseline of the PPG signal was removed in the preprocessing, the  $n_{OBi}$  and  $n_{EBi}$  points have similar amplitudes. Based on this, the range in which  $n_{EBi}$  was sought was restricted to the region of the pulse catacrotic phase with amplitude similar to  $\hat{x}_{PPG}(n_{OBi})$ . This region would not include neither the diastolic peak nor the dicrotic notch of the catacrotic phase, so filtering would not be necessary to soften the signal. Thus, overestimation and confusion between the dicrotic notch and the pulse end were avoided. This new methodology provides robust results in the estimation of the onset and end points, and a more accurate determination of the pulse width.

The pulse width, measured at base and half height of the pulse of the systolic peak, was considered. Previous works showed that the systolic amplitude and the pulse area correlate with the systemic vascular resistance worse than the pulse width at the half height of the systolic peak [18]. Significant differences were identified in the pulse width, measured at the base and at the half height of the systolic peak, in all the analysed stages except in  $\overline{PWB}$  for stage 5 (Fig. 4(a) and (b)), suggesting an increase in the systemic vascular resistance. However, a reduction in the ambient temperature can also produce this vasoconstriction, for this reason the temperature of the hyperbaric chamber was recorded during the test. Table I shows that a 4 atm increase in atmospheric pressure causes an increase in the ambient temperature around 3 °C. This increase in the temperature activates vasodilator system in the human body, and therefore more blood is transferred from the core to the surface of the skin [33]. However, our results show an increase in pulse width that other authors have related to a possible vasoconstriction [18]. A decrease in the distensibility of the arterioles could result in a longer time for the arterioles to reach the peak blood volume, that is, an increase in the pulse width. In fact, there is only one decrease of temperature inside the hyperbaric chamber, from 5 to 3A. The decrease in temperature

causes reflex activation of sympathetic vasoconstrictor nerves, resulting in cutaneous vasoconstriction and decrease blood flow to the skin [34]. This sympathetic activation is not observed in the  $P_{LFn}$  and  $R_{LF/HF}$  parameters (Fig. 3). The results of Fig. 4(a) and b, show an increase in the median value of  $\overline{PWB}$  and  $\overline{PWM}$  in stage 3A (only significant for  $\overline{PWM}$ ), with respect to the previous stages. The results do not allow us to discern whether this increase is due solely to the decrease in temperature or is also influenced by the increase in atmospheric pressure, with respect to the basal state. Regarding stage 1A, prior to this stage, subjects must perform decompression stops lasting between 50 and 55 minutes, allowing subjects to acclimatize to the small change in temperature, compared to the previous stage. The temperature changes between consecutive stages were significant, except between stages 3 A and 1 A. Based on these results, it can be ruled out that the increase in pulse width is due to a drop in temperature inside the chamber, except for stage 3A. Regarding the pulse amplitude, it did not show significant changes, except for a decrease in stage 1A respect 3D and 5 stages. This same effect in  $\overline{PA}$  was observed in subjects exposed to hyperbaric oxygen treatments [35], where subjects were exposed to oxygen partial pressures of at least 2 atm absolute. In our study, in the final ascent stages, several decompression stops were performed where the subjects were exposed, for a considerable period of time, to pressures that did not exceed 3 atm. It is in this period of time, where a decrease in  $\overline{PA}$  was observed. The work of Awad *et al.* [18], showed that an increase in the systemic vascular resistance is correlated with a decrease in pulse amplitude and an increase in pulse width, also observed in our results. Awad *et al.* [18] affirm that the pulse width increase is consistent with the prolongation of the time required for transmission of the pulse wave at the level of the arteriolar vessels due to the increased vascular resistance. This increase might be attributable to a vasoconstriction, or changes in blood viscosity [18]. Arteriolar resistance is under the control of the sympathetic nervous system. Vascular smooth muscle of arterioles is innervated primarily by the sympathetic nervous system. The reduction in arteriolar diameter (vasoconstriction) can increase the arteriolar resistance to blood flow [36]. It is known that in a hyperbaric environment, the increase in partial pressure of oxygen produces a general vasoconstriction (especially in kidneys, skeletal muscle, brain and skin) [9]. Therefore, sympathetic activity and temperature variations have an impact on peripheral blood flow [17], [37]. This sympathetic activation, however, was not observed in the frequency parameters of the PRV. In previous studies, the normalized power of the PRV in the LF band with respect to the sum of the powers of both LF and HF bands ( $P_{LFn}$ ), and the ratio between these two powers ( $R_{LF/HF}$ ) are considered as a representation of the sympathovagal balance of the ANS [2], [38], [39]. These parameters did not increase when the atmospheric pressure or the time in the hyperbaric environment augmented [2] (Fig. 3). Results even showed a significant decrease in the  $P_{LFn}$  and  $R_{LF/HF}$ , in stages 5 and 3A. This apparent discrepancy may be caused by the fact that the sympathetic activation was related to a vasoconstriction that do not affect the PRV frequency parameters. Based on this, it



can be considered that the decrease in  $\overline{PA}$  and the increase in pulse width was due to a vasoconstriction. The results seem to indicate that the PPG morphology allows the identification of an early sympathetic activation before this activation is intense enough to modify the frequency parameters of the PRV. Similar results were obtained in a previous study where low level of stress was induced in subjects [20]. However, in studies in which subjects were exposed to more demanding stressors (e.g. mental arithmetic, exams, reaction time), central sympathetic system was activated [38], [39]. It is not known whether an increase in the time of exposure to a hyperbaric environment or in the pressure reached, may cause a central sympathetic activation that modifies the PRV frequency parameters. More studies, with subjects exposed to higher pressures, are necessary to clarify the evolution of the ANS response.

In Fig. 4(a) and (b),  $\overline{PWB}$ ,  $\overline{PWM}$ ,  $\overline{PWB_d}$  and  $\overline{PWM_d}$  parameters show a similar trend with respect to the changes observed in the  $\overline{NN}$  parameter. However, the changes observed in parameters  $\overline{PWB_u}$  and  $\overline{PWM_u}$  are compatible with the expected physiological response in the subjects: an increase in vasoconstriction due to an increase in atmospheric pressure or a drop in temperature. It can be seen that these parameters increase with the increase in pressure (stages 3D and 5), and that in stage 3 A there was an increase in their values and greater interquartile ranges, due to the drop in temperature when going from stage 5 to 3 A. While the pressure increase was the same for all subjects, the change in temperature could not be adequately controlled between these two stages, which could cause the observed interquartile range increase. The vasoconstriction caused by the hyperbaric environment can be maintained for a few minutes, or hours, after returning to basal pressure [12], so the increase in  $\overline{PWB_u}$  and  $\overline{PWM_u}$  in stage 1A was also consistent with expectations. Even so, although there were indications that these parameters seem to be more suitable for identifying changes in the systemic vascular resistance than the pulse width, with the records performed in this work it cannot be guaranteed. The design of a specific test would be necessary to validate this point, which should include invasive measures of the systemic vascular resistance.

Regarding the ratios of the pulse width,  $\overline{PWB_r}$  and  $\overline{PWM_r}$  showed a significant decrease in all stages except for 1A. The trend of these parameters followed the pressure changes, and in stage 1A they recovered their baseline state. Although the width ratio was recovered in stage 1A, the width of both, the anacrotic phase and the catacrotic phase, increased significantly in this stage. The anacrotic phase is related to the systole [17] and the results showed significant increases in this phase ( $\overline{PWB_u}$  and  $\overline{PWM_u}$ ) at all stages. Regarding catacrotic phase, there were significant changes in  $\overline{PWB_d}$  at all stages, except in stage 5. However, the specific physiology of each subject can cause the dicrotic notch to be above the midline of the pulse or below. In those cases where the dicrotic notch falls below the midline,  $\overline{PWM_d}$  does not contain information from the reflected wave, but only from the systolic response.

As mentioned, exposure to a hyperbaric environment causes a general vasoconstriction and a bradycardia, but it can also

cause an increase in mean and diastole blood pressure, and an increase in the activity of cardiac parasympathetic nerves, which can be maintained after recovering the basal pressure of 1 atm [12]. The physiological response of subjects exposed to a hyperbaric environment is complex, and technical difficulties have prevented a comprehensive assessment of cardiovascular changes during diving in humans. Most of the knowledge on human diving physiology has been obtained from the study of head-out immersed subjects [40], [41]. Head-out immersion of humans in thermoneutral water causes an immediate translocation of blood from the limbs to the chest, as well as increased plasma volume due to transcapillary autotransfusion of fluid from the cells [8], which causes an increase in cardiac end-diastolic volume, stroke volume and cardiac output [8]. To compensate for these increases, a reflex autonomic response is caused which results in endocrine changes that try to return plasma volume and arterial pressure to pre-immersion levels. An increase in arterial blood pressure due to increased cardiac output can cause an increase in  $\overline{PA}$  [18]. As long as this increase in blood pressure is not recover to normal level, the increase in pulse amplitude would compensate for the decrease caused by vasoconstriction. This may be the reason for which a decrease in  $\overline{PA}$  is observed only in the final stages (3A and 1A), when the subject has already spent more than 45 min in a hyperbaric environment.

Wang *et al.* [19] split the pulse area at the dicrotic notch, according to wave reflection theory where an arterial blood pulse could be divided into two waves: a first wave produced by heart pumping and a second wave produced by pulse wave reflection. They found that the total peripheral resistance can be assessed by the ratio of the two areas. Therefore, the ratio between the areas of the second and first peaks in the PPG wave, is mainly influenced by the strength of the pulse wave reflection. Pulse wave reflection results from the mismatch between different parts in the arterial system. Other studies showed that approximately 90% of the total peripheral resistance is located in small arteries [19]. This is because if the small arteries contract, the total peripheral resistance will change, which will have an impact on the strength of the wave reflection, and will change the area ratio even more [19]. In the present work, the dicrotic notch of some subjects was not identifiable, so the pulse was divided into two areas separated by the maximum systolic point (areas of the anacrotic and catacrotic phases). In this case the area of the anacrotic phase (Fig. 2:  $PAB_u$ ) is a consequence of heart pumping, but the area of the catacrotic phase is a consequence of both heart pumping and pulse wave reflection (Fig. 2:  $PAB_d$ ). Therefore, this parameter is more generalizable, since the dicrotic notch can be difficult to locate.  $\overline{PAB_r}$  showed a significant decrease for all stages, except for stage 1A, which is consistent with an increase in peripheral resistance during the stages with increased atmospheric pressure. Nevertheless,  $\overline{PAM_r}$  did not show sufficient sensitivity to detect this increase in peripheral resistance. Additionally, the area under the PPG curve,  $\overline{PAB}$  and  $\overline{PAM}$ , increased with pressure, with no significant changes when baseline pressure was recovered in stage 1A. However, in a hyperbaric environment, there is not only an increase in

systemic vascular resistance, but there could also be an increase in cardiac output affecting  $\overline{PA}$ , and therefore also pulse areas. This may be the reason for the discrepancies observed in the 1A stage, between the pulse widths, which do not recover their reference state, and the calculated areas.

Regarding the pulse slopes, an increment in  $\overline{PS_d}$  can be observed while pressure increases, which was significant for stage 5, despite no significant changes were observed neither in  $\overline{PWB_d}$  nor in  $\overline{PA}$ . The decrease in  $\overline{PA}$ , in stage 1A, can be the origin of the decrease in  $\overline{PS_u}$  and  $\overline{PS_d}$ .  $\overline{PS_u}$  showed a greater sensitivity than  $\overline{PA}$  to change during the ascending stages (3A and 1A).

As mentioned above, in future work it would be interesting to include invasive measures of the systemic vascular resistance, but also measurement of the subjects blood pressure inside the hyperbaric chamber, which would imply that a physician should remain inside the hyperbaric chamber with the subjects.

## VI. CONCLUSION

The parameters extracted from the anacrotic phase of the pulse seem to follow the changes in atmospheric pressure better than the other morphological parameters. While the classical time and frequency parameters of PRV show an increase in parasympathetic activity ( $P_{HF}$ ) and a decrease in the parameters that characterize the sympathetic response ( $P_{LFn}$  and  $R_{LF/HF}$ ) in hyperbaric conditions, the morphological ones indicate a peripheral sympathetic activation. The peripheral activation produces a vasoconstriction that increases the pulse width and area. However, the pulse width of the anacrotic phase seems to be a better marker in the variation of peripheral vascular resistance than the pulse width. Future studies would be necessary to confirm this. Based on the results obtained, it seems that the morphology of the PPG signal could provide complementary information to that extracted from the PRV on the response of the cardiovascular and nervous systems of subjects exposed to hyperbaric environments, thus being a suitable tool for monitoring its activity in these environments. It is important to locate parameters that have a high correlation only with pressure changes, and are independent of the time elapsed in a hyperbaric environment, to simplify the future development of an automatic safety system for the diver's response to the hyperbaric environment. There were several parameters that seemed to maintain this relationship with pressure, such as:  $P_{HF}$ , pulse areas, and width ratios. However, the  $P_{HF}$  parameter needs a minimum of 4 minutes of recording and consecutive pulses to be extracted, but the morphological ones can be averaged over a few pulses that do not have to be consecutive. For this reason, the morphological parameters seem more optimal for the development of integrable applications in wearables like smart watches or bands.

## ACKNOWLEDGMENT

This work would never have been done without the collaboration of the *Hospital General de la Defensa en Zaragoza*, and the assistance as volunteers of the *Regimiento de Pontoneros y Especialidades de Ingenieros n° 12*.

## REFERENCES

- [1] K. T. Widmaier, E. P. Raff, and H. Strang, *Vander's Human Physiology: The Mechanisms Body Function*, 13th ed. McGraw-Hill Education, 2013.
- [2] A. Hernando *et al.*, "Autonomic nervous system measurement in hyperbaric environments using ECG and PPG signals," *IEEE J. Biomed. Health Inform.*, vol. 23, no. 1, pp. 132–142, Jan. 2019.
- [3] Task Force of the European Society of Cardiology the North American Society of Pacing and Electrophysiology, "Heart rate variability standards of measurement, physiological interpretation, and clinical use," *Circulation*, vol. 93, no. 5, pp. 1043–1065, 1996.
- [4] E. Barbosa, J. M. García-Manso, J. M. Martín-González, S. Sarmiento, F. J. Calderón, and M. E. Da Silva-Grigoletto, "Effect of hyperbaric pressure during scuba diving on autonomic modulation of the cardiac response: Application of the continuous wavelet transform to the analysis of heart rate variability," *Mil. Med.*, vol. 175, no. 1, pp. 61–64, 2010.
- [5] V. Lund, J. Laine, T. Laitio, E. Kentala, J. Jalonen, and H. Scheinin, "Instantaneous beat-to-beat variability reflects vagal tone during hyperbaric hyperoxia," *Undersea Hyperbaric Med.*, vol. 30, no. 1, pp. 29–36, 2003.
- [6] V. Lund, E. Kentala, H. Scheinin, J. Klossner, K. Sariola-Heinonen, and J. Jalonen, "Hyperbaric oxygen increases parasympathetic activity in professional divers," *Acta Physiol. Scand.*, vol. 170, no. 1, pp. 39–44, 2000.
- [7] Y. C. Lin and K. K. Shida, "Mechanisms of hyperbaric bradycardia," *Chin. J. Physiol.*, vol. 31, no. 1, pp. 1–22, 1988.
- [8] D. R. Pendergast and C. E. Lundgren, "The underwater environment: Cardiopulmonary, thermal, and energetic demands," *J. Appl. Physiol.*, vol. 106, no. 1, pp. 276–283, 2009.
- [9] C. R. Mortensen, "Hyperbaric oxygen therapy," *Current Anaesth. Crit. Care*, vol. 19, no. 5–6, pp. 333–337, 2008.
- [10] R. L. Sheridan and E. S. Shank, "Hyperbaric oxygen treatment: A brief overview of a controversial topic," *J. Trauma - Injury, Infection Crit. Care*, vol. 47, no. 2, pp. 426–435, 1999.
- [11] P. Barata, M. Cervaens, R. Resende, O. Camacho, and F. Marques, "Hyperbaric oxygen effects on sports injuries," *Ther. Adv. Musculoskel. Dis.*, Vol. 3, no. 2, pp. 111–121, 2011.
- [12] M. Kozakiewicz *et al.*, "Acute biochemical, cardiovascular, and autonomic response to hyperbaric (4 atm) exposure in healthy subjects," *Evidence-Based Complementary Alternative Med.*, vol. 2018, 2018.
- [13] M. Nitzan, A. Babchenko, B. Khanokh, and D. Landau, "The variability of the photoplethysmographic signal - A potential method for the evaluation of the autonomic nervous system," *Physiol. Meas.*, vol. 19, no. 1, pp. 93–102, 1998.
- [14] A. Schäfer and J. Vagedes, "How accurate is pulse rate variability as an estimate of heart rate variability?" *Int. J. Cardiol.*, vol. 166, no. 1, pp. 15–29, 2013.
- [15] S. Lu, H. Zhao, K. Ju, K. Shin, M. Lee, K. Shelley, and K. H. Chon, "Can photoplethysmography variability serve as an alternative approach to obtain heart rate variability information?" *J. Clin. Monit. Comput.*, vol. 22, no. 1, pp. 23–29, 2008.
- [16] N. Selvaraj, A. Jaryal, J. Santhosh, K. K. Deepak, and S. Anand, "Assessment of heart rate variability derived from finger-tip photoplethysmography as compared to electrocardiography," *J. Med. Eng. Technol.*, vol. 32, no. 6, pp. 479–484, 2008.
- [17] M. Elgendi, "On the analysis of fingertip photoplethysmogram signals," *Current Cardiol. Rev.*, vol. 8, no. 1, pp. 14–25, 2012.
- [18] A. A. Awad *et al.*, "The relationship between the photoplethysmographic waveform and systemic vascular resistance," *J. Clin. Monit. Comput.*, vol. 21, no. 6, pp. 365–372, 2007.
- [19] L. Wang, E. Pickwell-MacPherson, Y. P. Liang, and Y. T. Zhang, "Noninvasive cardiac output estimation using a novel photoplethysmogram index," in *Proc. 31st Annu. Int. Conf. IEEE Eng. Med. Biol. Soc.: Eng. Future Biomed., EMBC 2009*, 2009, pp. 1746–1749.
- [20] M. Peláez, M. T. Lozano, A. Hernando, M. Aiger, and E. Gil, "Photoplethysmographic waveform versus heart rate variability to identify low-stress states: Attention test," *IEEE J. Biomed. Health Inform.*, vol. 23, no. 5, pp. 1940–1951, Sep. 2019.
- [21] Y. Li, H. Yan, Z. Xu, M. Wei, B. Zhang, and Z. Shi, "Analysis of the changes in photoplethysmogram induced by exercise stress," *J. Med. Imag. Health Inform.*, vol. 3, no. 3, pp. 347–355, 2013.
- [22] S. P. Linder, S. M. Wendelken, E. Wei, and S. P. McGrath, "Using the morphology of photoplethysmogram peaks to detect changes in posture," *J. Clin. Monit. Comput.*, vol. 20, no. 3, pp. 151–158, 2006.
- [23] R. Pizov, A. Eden, D. Bystritski, E. Kalina, A. Tamir, and S. Gelman, "Arterial and plethysmographic waveform analysis in anesthetized patients with hypovolemia," *Anesthesiology*, vol. 113, no. 1, pp. 83–91, 2010.

- [24] M. D. Peláez-Coca, A. Hernando, C. Sánchez, M. T. L. Albalate, D. Izquierdo, and E. Gil, "Photoplethysmographic Waveform in Hyperbaric Environment," in *Proc. Annu. Int. Conf. IEEE Eng. Med. Biol. Soc., EMBS*, 2019, pp. 3490–3493.
- [25] D. Sokas, M. Gailius, and V. Marozas, "Diver physiology monitor and its graphical user interface," in *Proc. Int. Sci. - Practical Conf., Virtual Instrum. Biomed.*, 2016, pp. 5–9.
- [26] L. Sörnmo and P. Laguna, *Bioelectrical Signal Processing in Cardiac and Neurological Applications*. New York, NY, USA: Elsevier, 2005.
- [27] J. Lázaro, E. Gil, R. Bailón, A. Mincholé, and P. Laguna, "Deriving respiration from photoplethysmographic pulse width," *Med. Biol. Eng. Comput.*, vol. 51, no. 1–2, pp. 233–242, 2013.
- [28] E. Gil, J. M. Vergara, and P. Laguna, "Detection of decreases in the amplitude fluctuation of pulse photoplethysmography signal as indication of obstructive sleep apnea syndrome in children," *Biomed. Signal Process. Control*, vol. 3, no. 3, pp. 267–277, 2008.
- [29] J. Lázaro, E. Gil, J. M. Vergara, and P. Laguna, "Pulse rate variability analysis for discrimination of sleep-apnea-related decreases in the amplitude fluctuations of pulse photoplethysmographic signal in children," *IEEE J. Biomed. Health Inform.*, vol. 18, no. 1, pp. 240–246, 2014.
- [30] E. Peralta, J. Lazaro, R. Bailon, V. Marozas, and E. Gil, "Optimal fiducial points for pulse rate variability analysis from forehead and finger photoplethysmographic signals," *Physiol. Meas.*, vol. 40, no. 2, 2019, Art. no. 025007.
- [31] R. Bailón, G. Laouini, C. Grao, M. Orini, P. Laguna, and O. Meste, "The integral pulse frequency modulation model with time-varying threshold: Application to heart rate variability analysis during exercise stress testing," *IEEE Trans. Biomed. Eng.*, vol. 58, no. 3, pp. 642–652, Mar. 2011.
- [32] R. Bailón, L. Sörnmo, and P. Laguna, "A robust method for ECG-based estimation of the respiratory frequency during stress testing," *IEEE Trans. Biomed. Eng.*, vol. 53, no. 7, pp. 1273–1285, 2006.
- [33] N. Charkoudian, "Mechanisms and modifiers of reflex induced cutaneous vasodilation and vasoconstriction in humans," *J. Appl. Physiol.*, vol. 109, no. 4, pp. 1221–1228, 2010.
- [34] D. W. DeGroot and W. L. Kenney, "Impaired defense of core temperature in aged humans during mild cold stress," *Amer. J. Physiol. - Regulatory Integrative Comparative Physiol.*, vol. 292, no. 1, pp. R103–R108, 2007.
- [35] T. Chonis and J. S. Cooper, *Hyperbaric, Cardiovascular Effects*, 2018. [Online]. Available: <http://www.ncbi.nlm.nih.gov/pubmed/29489293>
- [36] G. D. Thomas, "Neural control of the circulation," *Amer. J. Physiol. - Adv. Physiol. Educ.*, vol. 35, no. 1, pp. 28–32, 2011.
- [37] F. Heyman and N. E. Ahlberg, "Effect of rapid distension of large arteries and veins on the vascular tone of the fingers," *Acta Medica Scand.*, vol. 183, no. 1–6, pp. 337–340, 1968.
- [38] A. Hernando *et al.*, "Inclusion of respiratory frequency information in heart rate variability analysis for stress assessment," *IEEE J. Biomed. Health Inform.*, vol. 20, no. 4, p. 1, 2016.
- [39] G. G. Berntson, J. T. Cacioppo, and A. Fieldstone, "Illusions, arithmetic, and the bidirectional modulation of vagal control of the heart," *Biol. Psychol.*, vol. 44, pp. 1–17, 1996.
- [40] G. O. Dahlback, E. Jonsson, and M. H. Liner, "Influence of hydrostatic compression of the chest and intrathoracic blood pooling on static lung mechanics during head out immersion," *Undersea Biomed. Res.*, vol. 5, no. 1, pp. 71–85, 1978.
- [41] K. Shiraki, N. Konda, S. Sagawa, Y. C. Lin, and S. K. Hong, "Cardiac output by impedance cardiography during head-out water immersion," *Undersea Biomed. Res.*, vol. 13, no. 2, pp. 247–256, 1986.